scientific reports

Check for updates

OPEN

# Unveiling the dual-state emissive behaviour of 4,6-diarylpyrimidin-2-amines through a plug-and-play approach

Ajil R. Nair[1], M. Gayathri Mohan[2], C. Raksha[1], Anjana Sreekumar[1], P. Manoj[2], Y.C. Sunil Kumar[3] & Akhil Sivan[1]✉

**We present here a series of 4,6-diarylpyrimidin-2-amine derivatives (5a-j) with tunable optical properties both in the solid and solution states. Our plug-and-play fluorophore design demonstrates that the aryl groups at the 4th and 6th positions of the 2-aminopyrimidine core enable distinct optical characteristics for each derivative. The fluorophore design concept was validated using theoretical and spectroscopic methods. The designed compounds were synthesised in moderate to good yields, and their structures were confirmed *via* IR, NMR, HRMS, and single-crystal XRD analyses. Optical studies revealed that varying the aryl substituents significantly impacts absorption, emission, and bandgap values in both phases. The absolute quantum yields ($\phi_F$) of the synthesised derivatives ranged from 8.11 to 71.00% in DMF and 5.86–29.43% in thin films, with fluorescence lifetimes (τ) between 0.8 and 1.5 ns in DMF and 0.63–3.16 ns in films, respectively. CIE (Commission Internationale de l'Éclairage) diagrams indicate blue-green emission for 5a-j in the visible spectrum. The electrochemical analysis confirmed that the HOMO/LUMO (Highest Occupied Molecular Orbital/Lowest Unoccupied Molecular Orbital) energy levels can be modulated by altering the substituent rings. These results highlight the dual-state emission properties of 2-aminopyrimidine fluorophores, demonstrating their potential for a wide range of optoelectronic and advanced applications.**

**Keywords** CIE, Fluorophores, HOMO-LUMO, Optical bandgap, 2-aminopyrimidine, 4, 6-diarylpyrimidin-2-amine

Photoluminescence, the emission of light from excited electronic states after light absorption, has numerous applications in science and technology, which include fluorescence microscopy, lighting and display, forensics, fluorescent and phosphorescent dyes, phosphorescent cyphers, and counterfeit detection for security documents and artwork[1,2]. Fluorescence, a popular photoluminescence mechanism, dates back to the 19th century when a German chemist, Adolf von Baeyer, synthesised the first fluorophore pigment in 1871[3]. Since then, research on the design and development of unique fluorophores has become significant. Conjugated small organic fluorophores have advantages such as being lightweight, flexible, easy to synthesise, and inexpensive, making them popular as potential luminous materials[4]. Applications such as organic light-emitting diodes (OLED), bio-imaging, fluorometric sensors, and fluorescence microscopy recognise fluorescent organic molecules as notable candidates[5–8]. However, there are limited references available for the design and synthesis of suitable fluorophores for specific needs, and the selection of these requires the expertise of the researchers involved[9].

Heterocyclic molecular systems are valuable components of fluorophores, offering diverse photophysical properties and applications[10–12]. These heterocycles serve as electron donors, acceptors, and spacer groups and also contribute to the optical properties of the molecules[13]. Factors such as lone pairs of electrons, aromatic character, electronegativity of heteroatoms in the ring, extended conjugation, and delocalisation of the π-electrons contribute to their versatility and tunable optical characteristics. Recent literature on heterocycle-based small organic fluorophores and the influence of trivial structural modifications on their photophysical characteristics echo the scope of future research[14–16]. Pyrimidine is a two-nitrogen-containing member of the heterocyclic

[1]Department of Chemistry, Amrita Vishwa Vidyapeetham, Amritapuri 690525, Kollam, Kerala, India. [2]Department of Chemistry, St. Michael's College, Cherthala 688539, Kerala, India. [3]Department of Chemistry, Dayananda Sagar Academy of Technology and Management, Udayapura, Kanakapura Road, Bengaluru 560082, Karnataka, India. ✉email: akhilsivan@am.amrita.edu

family and is found in natural products and synthesised chemicals[17–19]. Pyrimidine derivatives are crucial in creating physiologically active substances and complex chemicals. Various pyrimidine-cored organic molecules have exceptional photophysical properties and operate as OLED components[20–23]. In the present study, we have designed and synthesised ten fluorophores (**5a-j**), each having a 2-aminopyrimidine core. These fluorophores have various combinations of thiophene, furan, pyrrole, and phenyl rings at the 4$^{th}$ and 6$^{th}$ positions of the pyrimidine ring. The synthesis and biological activities of many 4, 6-diarylpyrimidin-2-amine derivatives are explored and well documented[24–27], however, their photophysical and electrochemical properties have not been reported.

Recent literature reports indicate that modifying hetero atoms and substituents (groups with electron-donating or electron-withdrawing effects) in the skeletal structure has a substantial impact on the photophysical and electrochemical features of fluorophores. We altered the 4$^{th}$ and 6$^{th}$ positions of the synthesised fluorophores by employing various aromatic groups such as phenyl, thienyl, furyl, and pyrrolyl rings to achieve unique photophysical characteristics for each corresponding derivative. Moreover, in the area of advanced organic synthesis, the scope of synthesising a wide variety of compounds from an aminopyrimidine moiety is huge. They can undergo nucleophilic substitution reactions due to the presence of the nucleophilic amino group (-$NH_2$), react with carbonyl compounds to form imines, and with carboxylic acids or their derivatives to form amides. Additionally, the amino group can be oxidised to produce nitro compounds and other oxidised derivatives. By diazotising the -$NH_2$ group followed by performing coupling reactions such as C-N or Buchwald-Hartwig[28], complexes with transition metals can be formed. One can deliberately employ the aforementioned strategies to modify the optical properties of 4, 6-diarylpyrimidin-2-amine derivatives for future investigations.

The goal of this study is to look into a "plug-and-play" method for creating 4, 6-diarylpyrimidin-2-amines. The core pyrimidine structure acts as a flexible framework that lets different aromatic groups (like thiophene, furan, pyrrole, and phenyl) be added at the 4$^{th}$ and 6$^{th}$ positions. Here the 'plug-and-play' approach refers to maintaining the core pyrimidine structure unchanged while selectively altering the 4$^{th}$ and 6$^{th}$ positions through various aryl group substitutions. This modular strategy enables the fine-tuning of emission properties without altering the overall molecular framework. By adjusting the electronic and steric characteristics of these substituents, we can easily control the HOMO-LUMO energy gap as well as their photophysical behaviour. The "plug-and-play" fluorophore design makes them highly adaptable for a wide range of applications and offers a high scope of future research on fluorophores with similar architecture. This work can be considered the first of its kind, demonstrating the flexible optical properties of small organic fluorophores having a 2-aminopyrimidine core.

We conducted theoretical verification for the design concept of 4, 6-diarylpyrimidin-2-amine fluorophores utilising Gaussian 09 W software and validated the design concept. The overall photophysical properties of compounds **5a-j** exhibited distinctive optical properties both in solution (DMF) and solid (thin film) phases. These results imply that the modification of the aromatic substituents at the 4$^{th}$ and 6$^{th}$ positions of the 2-aminopyrimidine core has had a substantial impact on the optical properties of compounds **5a-j**, both in solution and in the solid form. The fluorophore **5b** displayed the highest quantum yield of 71% in the solution phase and 29.43% in thin film. Factors such as local environmental conditions, molecular mobility and rotation in the solution phase, restricted molecular rotation in the solid phase, and efficient π-π stacking in the solid phase are responsible for the dual-state optical properties of the target compounds. Most importantly, it is seen that dual-state emissive molecules, which exhibit unique emissions both in the solid and solution states, are highly preferred to be used in a wide range of domains, including optoelectronics[29,30], biomedical imaging[31], and chemical sensors[32,33]. Cyclic voltammetry (CV) experiments have also confirmed the manipulation of the HOMO/LUMO energy levels of 2-aminopyrimidines by altering the aryl rings at the 4$^{th}$ and 6$^{th}$ positions. This provides convincing proof for the unique electronic environment of the target molecules. The present study ultimately aims to demonstrate novel and innovative core architecture that exhibits dual emission behaviour for future applications. We believe that these compounds hold great promise for further exploration and practical applications in diverse fields, making them captivating subjects for future research and innovation.

## Results and discussion

### X-ray crystallographic results

The single crystal XRD analysis of a representative compound **5e** confirmed its planar structure. The brown crystals having a size of 0.400 × 0.300 × 0.200 mm were formed by allowing **5e** to slowly evaporate from a solution in acetonitrile solvent over a period of 20 days. Figure 1a depicts the crystal structure of **5e**. Single-crystal X-ray studies revealed the compound's orthorhombic crystalline structure with a P 21 21 21 space group. The SI section (**SI** Table 1 and **SI** Figs. 1 and 2) provides the comprehensive single crystal XRD data and structure parameters of **5e**.

Figure 1b and **SI** Fig. 3 respectively display the molecular packing and interactions of **5e**, generated using CCDC Mercury software. **SI** Fig. 3 confirms the perfect planar geometry of **5e**, and the packing diagram illustrates how the conjugated planes interact. Planar molecules like **5e** often exhibit significant π-π stacking interactions between aromatic rings, which play a critical role in determining the solid-state photophysical properties. Figure 1b indicates the absence of intramolecular interactions, but the crystal structure displays valid intermolecular interactions. Notably, the sulphur atom (S2) forms a strong hydrogen bond with nitrogen-bound hydrogen (H3B—N3), represented as S2····H3B—N3 (2.858 Å). Additionally, classic N-H····N hydrogen bonds are present, including N1····H3A—N3 (2.268 Å) and N2····H3B—N3 (2.325 Å). These intermolecular interactions stabilise the molecular arrangement, rigidify the framework, and prevent intramolecular rotations, contributing to the enhanced solid-state properties of **5e**.

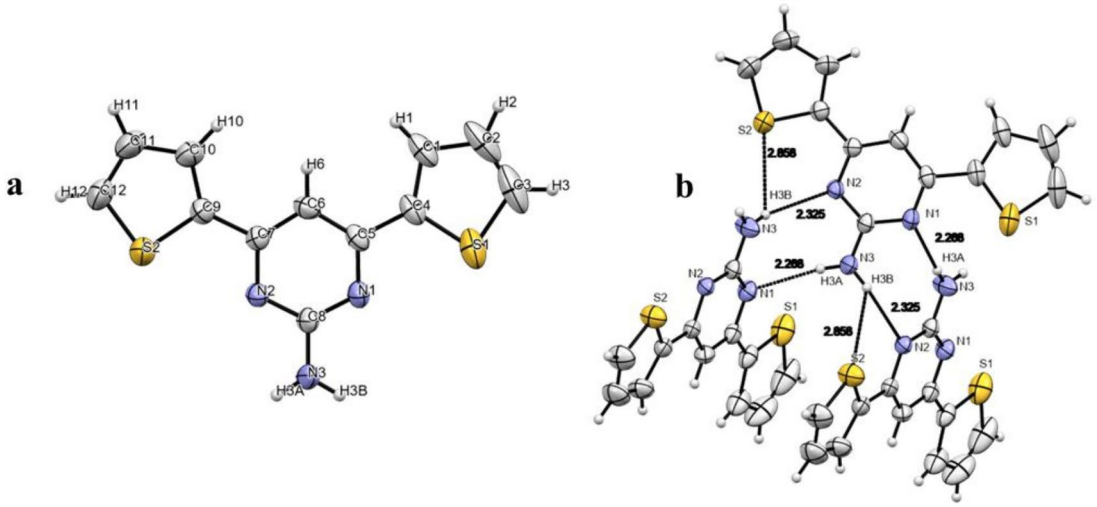


**Fig. 1**. (**a**) ORTEP diagram of **5e**, (**b**) Intermolecular interactions in **5e**.

| Compound | HOMO (eV) | LUMO (eV) | Energy Gap/ΔE (eV) |
|---|---|---|---|
| **5a** | − 6.2586 | −1.8503 | 4.40 |
| **5b** | − 6.1497 | −1.9755 | 4.17 |
| **5c** | − 5.7824 | −1.4748 | 4.30 |
| **5d** | − 5.8450 | −1.7007 | 4.14 |
| **5e** | − 6.1062 | −2.0599 | 4.04 |
| **5f** | − 5.8450 | −1.8721 | 3.97 |
| **5g** | − 5.7443 | −1.5945 | 4.15 |
| **5h** | − 6.0109 | −1.8639 | 4.14 |
| **5i** | − 5.8096 | −1.7252 | 4.08 |
| **5j** | − 5.7688 | −1.5374 | 4.23 |

**Table 1**. Calculated HOMO-LUMO orbital energy and bandgap (ΔE) values of **5a-j**.

## Computational studies

Theoretical validation of the fluorophore design (plug-and-play approach) was done utilising Gaussian 09 W software (refer to **Sect. 4.1** for experimental details). We performed the structure optimisation and HOMO-LUMO energy calculations in the gas phase. The ground-state optimised structure and HOMO-LUMO diagram of **5a-j** are shown in Fig. 2 and **SI** Fig. 4, respectively.

The HOMO and LUMO orbitals of the symmetric compounds **5a**, **5e**, **5 h**, and **5j** and the unsymmetrical compound **5g** are uniformly distributed across the entire molecular framework, suggesting a $\pi \rightarrow \pi^*$ transition mechanism. In the case of 2-aminopyrimidine derivatives with one phenyl and one hetero-aromatic substituent **(5b-5d)**, the HOMO orbitals are shifted towards the electron-rich hetero-aromatic ring and 2-aminopyrimidine ring, whereas the LUMO orbitals are evenly distributed among the three aromatic rings. For the compounds **5f** (having thiophene and pyrrole rings) and **5g** (having furan and pyrrole rings), both the $4^{th}$ and $6^{th}$ positions of the 2-aminopyrimidine ring are occupied by hetero-aromatic rings. Here, the LUMO orbitals are evenly distributed across the skeletal structure, whereas the HOMO orbitals are shifted towards the pyrrole ring, which indicates a high electron density on the pyrrole ringside. The shift in HOMO/LUMO orbitals on changing the substituent rings at the $4^{th}$ and $6^{th}$ positions of the 2-aminopyrimidine ring is evident from the computed energy gap (ΔE). Table 1 provides a summary of the calculated HOMO-LUMO orbital energy value and ΔE values for **5a-j**. The calculated energy gap varies between 3.97 eV and 4.40 eV; the highest ΔE values are found for **5a** (4.40 eV), **5c** (4.30 eV), and **5j** (4.23 eV), and the rest of the compounds have comparable ΔE values. Interestingly, the compounds (**5b-5d**, **5f**, and **5g**) have HOMO orbitals distributed only on the electron-rich hetero-aromatic rings, whereas the LUMO orbitals are distributed throughout the molecular structure. This phenomenon leads to the crucial occurrence of the intramolecular charge transfer (ICT) mechanism. The overall computational results confirm the possibility of bandgap engineering of the 2-aminopyrimidine derivatives achieved *via* the plug-and-play approach.

The absorption behaviour of compounds **5a-j** was theoretically studied in ten different solvents, ranging from the least polar toluene to the highly polar dimethylsulphoxide (DMSO), using the TD-SCF (Time-dependent

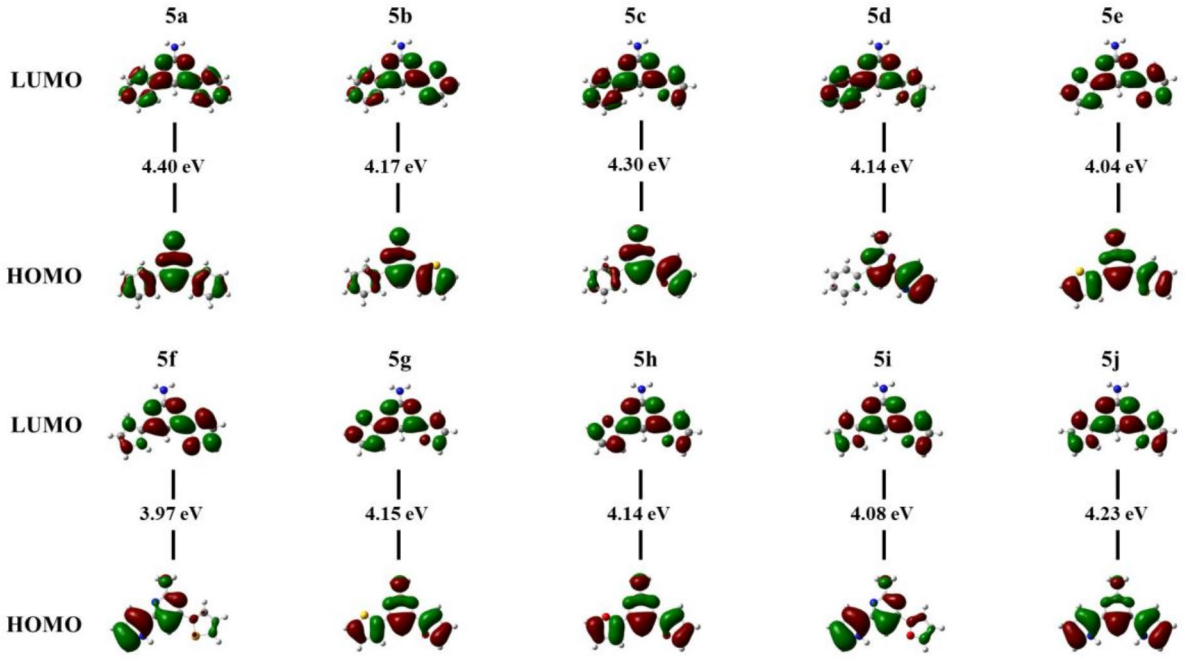


**Fig. 2**. Frontier molecular orbitals (FMOs) and the calculated bandgap (ΔE) values of **5a-j**.

Hartree-Fock and density-functional theory) method. The analysis focused on investigating the impact of solvent polarity on the absorption properties[34]. **SI** Fig. 5a-j displays the theoretical UV-visible spectrum of compounds **5a-j** in various solvents, and the unique absorption behaviour of the studied compounds is revealed here. **SI** Table 2 presents the comprehensive theoretical absorption characteristics. Except for DMF and ethyl acetate, most compounds exhibited multiple absorption peaks in the solvents that were examined. No noticeable trend in the shift of absorption maxima or bandgap values is observed on increasing the solvent's polarity from toluene to DMSO. However, we calculated the least bandgap in the extremely polar solvents, DMF and DMSO, compared to other selected solvents.

## Photophysical studies

The core moiety (2-aminopyrimidine) remains the same for the compounds **5a-j**, but the aryl groups in the $4^{th}$ and $6^{th}$ positions are varied to aim for their unique optical characteristics. The order of aromaticity of hetero-aromatic rings and the electronegativity of heteroatoms can contribute to their optical characteristics. We studied the absorption and emission behaviour of the target compounds (**5a-j**) both in solution and thin film samples to evaluate these. Since the core structure of the synthesised fluorophore derivatives is the same, the solvatochromism studies of two representative products, **5e** and **5g**, in ten different solvents (**SI** Figs. 6–9) were carried out. The absorption and emission spectra showed a slight shift in absorbance ($\lambda_{abs}$) and emission ($\lambda_{em}$) maximums with increasing solvent polarity. Polar solvents such as *N*, *N*-dimethylformamide (DMF) and DMSO showed higher absorbance and emission maximum for **5e** and **5g** compared to non-polar solvents. The bathochromic shift in highly polar solvents occurs when the excited state is more polar than the ground state. The polar solvents preferentially stabilise the excited state, thereby reducing the energy difference with the ground state leading to a shift towards longer wavelengths. **SI** Table 3 summarises the effect of solvent polarity on the absorption and emission maximum of **5e** and **5g**. The solvent DMF was chosen further for the solution state photophysical studies based on the observed $\lambda_{abs}$ and $\lambda_{em}$ values of **5e** and **5g** as well as the solubility of **5a-j** in the selected solvents. The UV-visible and PL spectroscopy studies insights into the electronic structure of the organic compounds being studied. **Section 4.1** details the sample preparation for UV-visible and PL studies.

Fig. 3a and b display the UV-visible and PL spectra of **5a-j** in solution (DMF), respectively. Two characteristic absorption peaks at 263–290 nm and 342–364 nm are observed for these compounds, possibly due to multiple electronic transitions ($\pi \rightarrow \pi^*$ and $n \rightarrow \pi^*$) and charge transfer mechanisms (ICT) upon absorbing UV-visible radiation. The optical bandgap in solution ($\Delta E_s$) for the target compounds **5a-j** is calculated *via* the Tauc plot method, and the results are summarised in Table 2. The Tauc plots corresponding to each target are displayed in **SI Fig. 10**. The highest bandgap value was recorded for **5a** (4.37 eV) with two phenyl substituents and the lowest for **5b** (3.94 eV) with thienyl and phenyl substituents, both in DMF solution. For the compounds **5a**, **5d-5f**, **5h**, and **5i**, theoretically calculated bandgap (ΔE) and experimentally calculated bandgap in solution ($\Delta E_s$) values are comparable, and for the other compounds (**5b**, **5c**, **5g**, and **5j**), the difference between ΔE and $\Delta E_s$ values are only between 0.12 and 0.26 eV.

Conjugation, delocalisation, and electron-donating/withdrawing substituents significantly affect the energy gap between the HOMO and LUMO. The aromatic conjugated systems with perfect delocalisation lower the

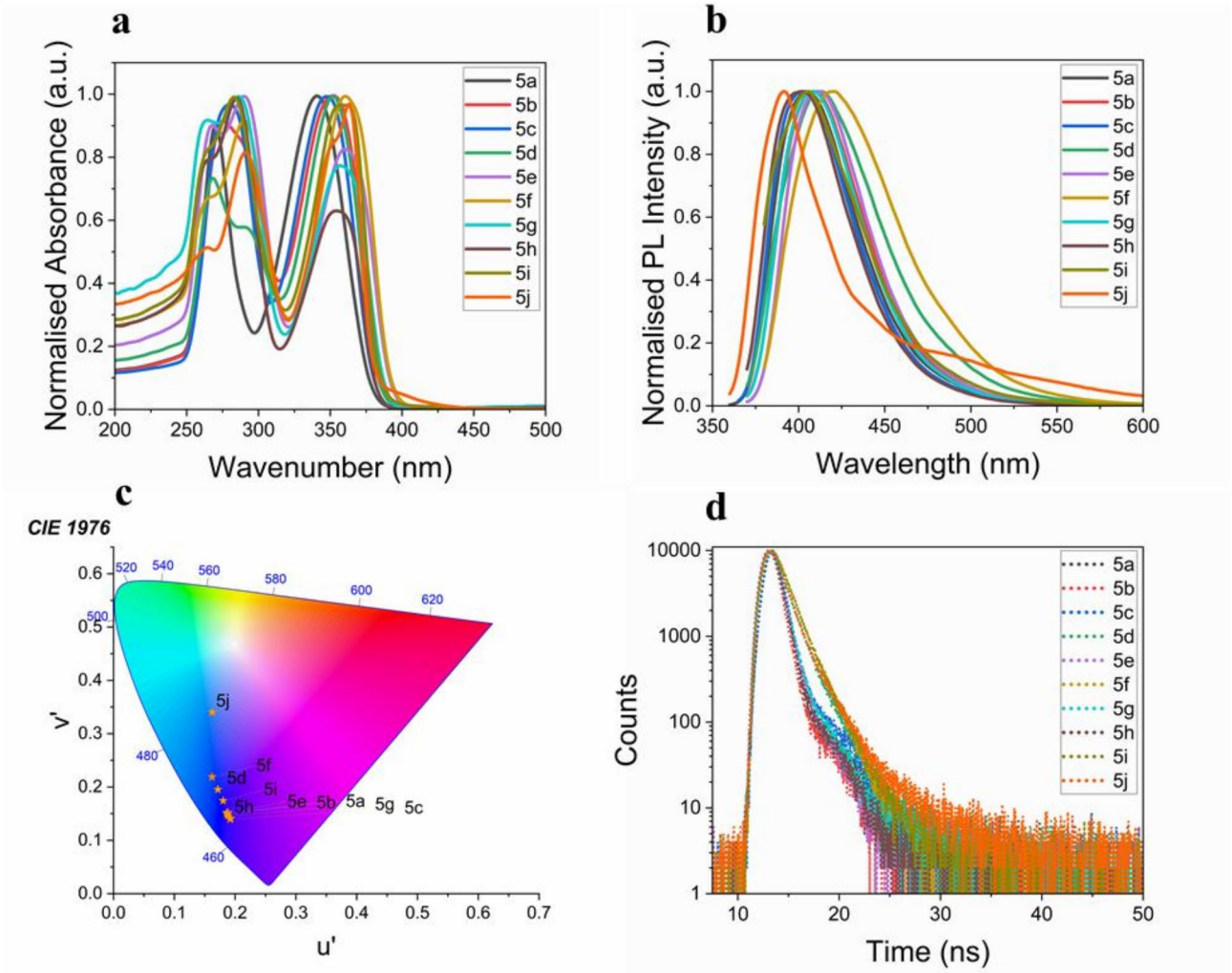


**Fig. 3**. (**a**) Normalised UV-visible spectrum, (**b**) Normalised PL spectrum, (**c**) CIE plot w.r.t. PL data, and (**d**) Fluorescence lifetime curve of **5a-j** in DMF.

energy gap between the HOMO and LUMO, resulting in a smaller energy gap. An electron-donating group can increase the electron density on the aromatic ring and raise the energy level of HOMO, which facilitates the lowering of the HOMO-LUMO gap; similarly, electron-withdrawing atoms/groups can decrease the bandgap by lowering the energy levels of LUMO[17,18]. In the present case, **5a** (phenyl groups at the 4$^{th}$ and 6$^{th}$ positions of 2-aminopyrimidine) has the highest $\Delta E_s$ of 4.37 eV compared to all other derivatives. The non-bonded pair of electrons on the thiophene/furan/pyrrole ring contributes to the conjugation of the other nine derivatives, which have one or two hetero-aromatic rings on the 2-aminopyrimidine ring. This conjugation increases electron delocalisation and lowers the HOMO-LUMO gap, resulting in lower $E_s$ for **5b**-**5j** compared to **5a**. For the hetero-aryl substituted symmetric compounds (**5e**, **5h**, and **5j**), the lowest bandgap is observed for **5j** (3.97 eV, containing a pyrrole ring), followed by **5e** (4.03 eV, containing a thiophene ring), and **5h** (4.08 eV, containing a furan ring). This order is influenced by the superior electron-donating ability of pyrrole, the larger atomic size of sulphur in thiophene, and the high electronegativity of oxygen in furan, each affecting the compounds' electronic environments. The calculated $E_s$ values for the other set of unsymmetric compounds show no clear trend. The varied combinations of substituent rings create a diverse electronic environment for each molecular structure, resulting in unique bandgap values. Table 2 summarises the $E_s$ results. In dilute solutions, molecular motion, rotation, and distorted planarity can significantly impact $\Delta E_s$ values, potentially reducing conjugation effectiveness and contributing to the irregular trends observed in the $\Delta E_s$ results.

According to Fig. 3b, all compounds (**5a-j**) have a single emission peak, with the $\lambda_{em}$ observed at 393–421 nm in the violet region. A 28 nm difference is observed between **5j** (393 nm) of high energy emission and **5f** (421 nm) of low energy emission. The closeness in $\lambda_{em}$ values indicates that the fine-tuning of emission colour is achieved for the 2-aminopyrimidine-cored fluorophores in the solution phase. The emission peak is broader within the range of 180–240 nm and covers a violet-to-green region of the visible light. According to the CIE plot (Fig. 3c), the emission colour of **5a-j** is in the violet-blue region, and the closeness in CIE coordinate values further confirms the fine-tuned emission colour in DMF. The concentration of compounds **5a-j** in DMF is adjusted to

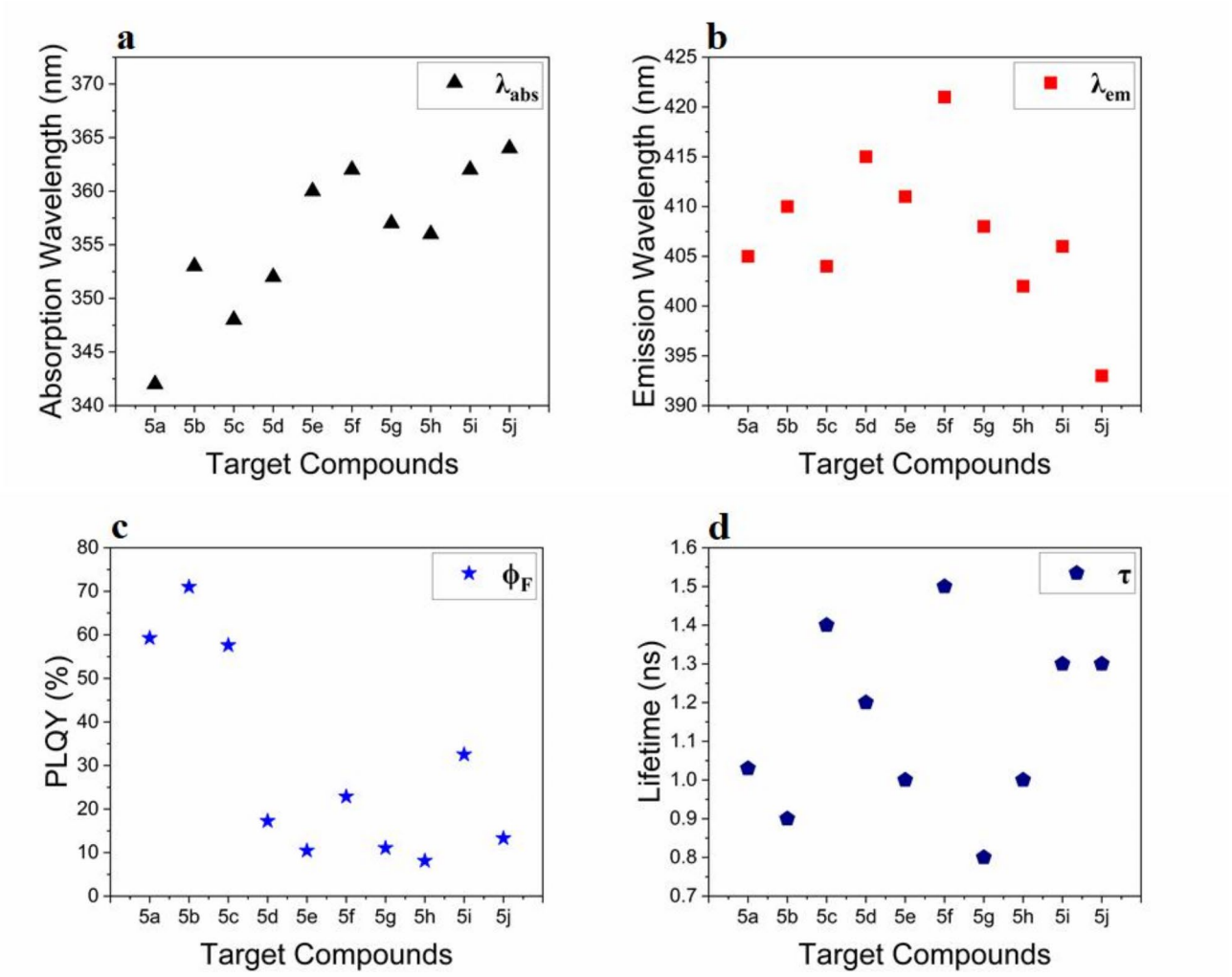


**Fig. 4**. Variations of (**a**) absorption maximum, (**b**) emission maximum, (**c**) absolute PLQY, and (**d**) fluorescence lifetime of **5a-j** in DMF solvent.

make the absorbance ≈ 1, and the absolute PLQY ($\phi_F$) and fluorescence lifetime/LT ($\tau$) are also measured. The obtained $\phi_F$ for **5a-j** is between 8.11 and 71.00%. Among the ten target compounds, the highest $\phi_F$ is observed for **5b** (71.00%) and the lowest is for **5h** (8.11%). The compounds **5a** (59.26%), **5c** (57.60%), **5i** (32.51%), and **5f** (22.85%) also displayed moderate to good $\phi_F$ which is a valid proof showing the emission efficiency of the demonstrated fluorophore class. A PLQY greater than 20% indicates that at least one-fifth of the absorbed photons are re-emitted as fluorescence, making them suitable for various applications where extremely high brightness is not so crucial. Among all the synthesised molecules, compounds **5a** (59.26%), **5b** (71.00%), and **5c** (57.60%), which contain one or two phenyl substituents, exhibit the highest $\phi_F$ values. In these compounds, the potential for both intramolecular and intermolecular hydrogen bonding is minimal, which helps maintain their emission efficiency. In contrast, compounds **5d**-**5j** may experience increased intramolecular and intermolecular interactions (due to the presence of electronegative hetero atoms) that favour non-radiative decay pathways and energy transfer to non-emissive states, ultimately reducing their PLQY in solution. The fluorescence lifetime ($\tau$) refers to the precise time during which a molecule remains in its excited state before coming back to the ground state. The fluorescence lifetime curve of **(5a-j)** is shown in Fig. 3d, and the $\tau$ values usually fall within the nanosecond (ns) range. The measured $\tau$ value of **5a-j** is between 0.8 and 1.5 ns, for which the majority of the compounds showed $\tau \geq 1$ ns, barring compounds **5b** (0.9 ns) and **5g** (0.8 ns), both demonstrated the least. Table 2 provides a summary of the photophysical characteristics of compounds **5a-j** in DMF solvent. Figure 4a-d depicts the variations in absorption maximum, emission maximum, absolute PLQY, and fluorescence lifetime among compounds **5a-j** in the solution phase.

We recorded the absorption and emission behaviour of the thin films of **5a-j** and displayed the spectrum in Fig. 5a and b, respectively. Figure 5a shows a single broad absorption peak for the film samples, and the absorbance maximum ($\lambda_{abs}$) is located at 344–374 nm. Compared to the solution, the film sample's absorption peak became slightly broader, and the $\lambda_{abs}$ seemed slightly redshifted. Several factors contribute to these changes. In the solid phase, the molecules are often closer to each other, leading to strong intermolecular interactions like $\pi$-$\pi$ stacking. This interaction can cause a wider distribution of energy levels and also affect the electronic

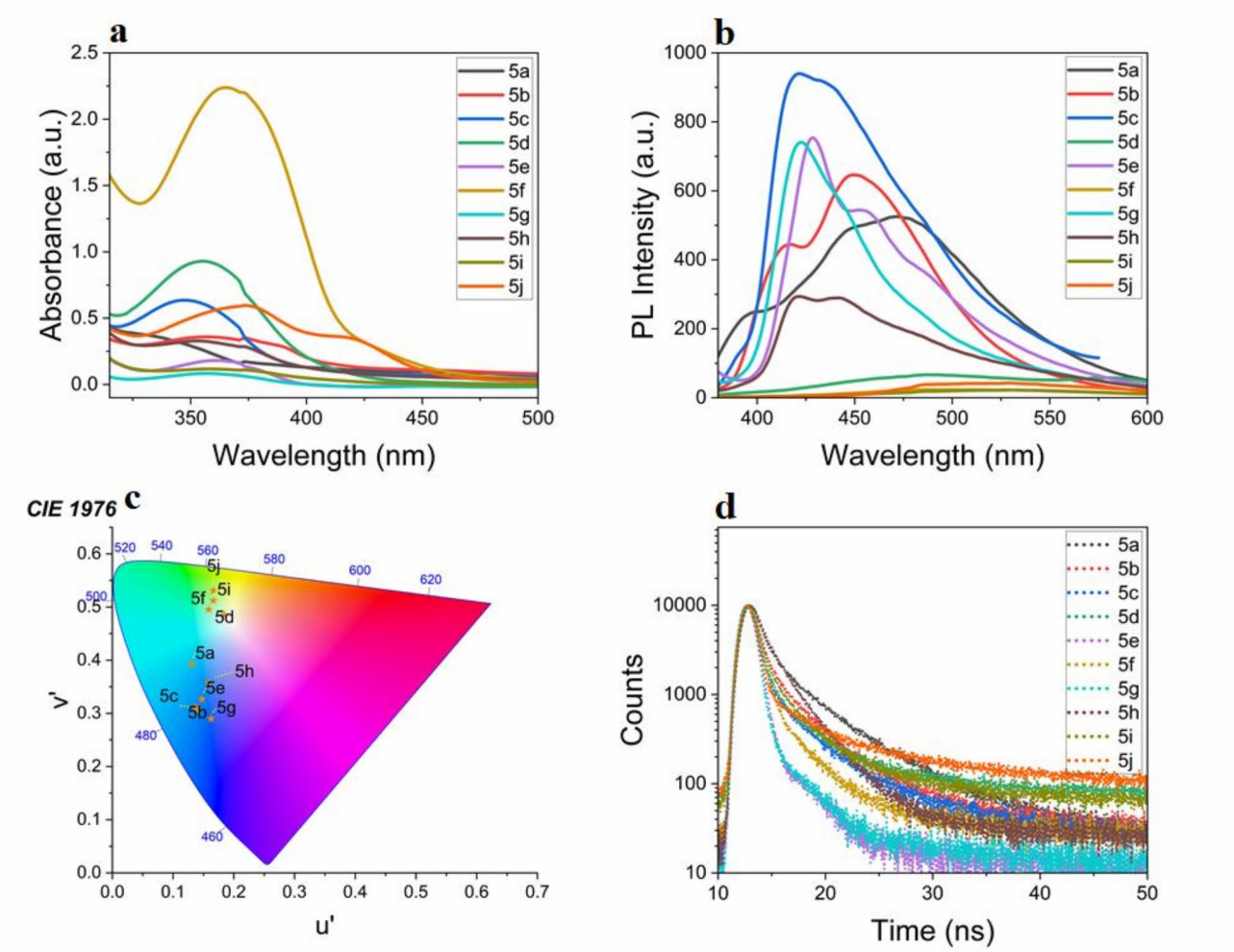


**Fig. 5**. (**a**) UV-visible spectrum, (**b**) PL spectrum, (**c**) CIE plot w.r.t. PL data, and (**d**) Fluorescence lifetime curve of **5a-j** film.

| Compound | UV $\lambda_{abs}$ (nm) | Excitation (nm) | PL $\lambda_{em}$ (nm) | $\lambda_{Onset}$ (nm) | $\Delta E_s$ (eV) | CIE (u', v') | $\phi_F$ (%) | τ (ns) |
|---|---|---|---|---|---|---|---|---|
| **5a** | 342 | 340 | 405 | 377 | 4.37 | 0.21, 0.06 | 59.26 | 1.3 |
| **5b** | 353 | 350 | 410 | 390 | 3.94 | 0.21, 0.06 | 71 | 0.9 |
| **5c** | 348 | 350 | 404 | 381 | 4.09 | 0.21, 0.06 | 57.6 | 1.4 |
| **5d** | 352 | 350 | 415 | 385 | 4.15 | 0.20, 0.07 | 17.25 | 1.2 |
| **5e** | 360 | 360 | 411 | 395 | 4.03 | 0.21, 0.07 | 10.43 | 1 |
| **5f** | 362 | 360 | 421 | 394 | 3.97 | 0.19, 0.10 | 22.85 | 1.5 |
| **5g** | 357 | 360 | 408 | 399 | 4.03 | 0.21, 0.07 | 11.04 | 0.8 |
| **5h** | 356 | 360 | 402 | 389 | 4.08 | 0.21, 0.06 | 8.11 | 1 |
| **5i** | 362 | 360 | 406 | 390 | 4.05 | 0.20, 0.08 | 32.51 | 1.3 |
| **5j** | 364 | 365 | 393 | 384 | 3.97 | 0.19, 0.10 | 13.29 | 1.3 |

**Table 2**. The overall photophysical characteristics of **5a-j** in DMF solvent.

transitions, resulting in broader absorption peaks and redshifted $\lambda_{abs}$. Additionally, the restricted molecular motion/rotation in the solid phase can lead to a more planar conformation, also adding up to the above-mentioned wavelength shift.

The optical bandgap ($\Delta E_F$) for the compounds **5a-j** in the solid state was calculated *via* the Tauc plot method (**SI Fig. 11**), and the results are summarised in Table 3. As a consequence of the abovementioned factors, $\Delta E_F$

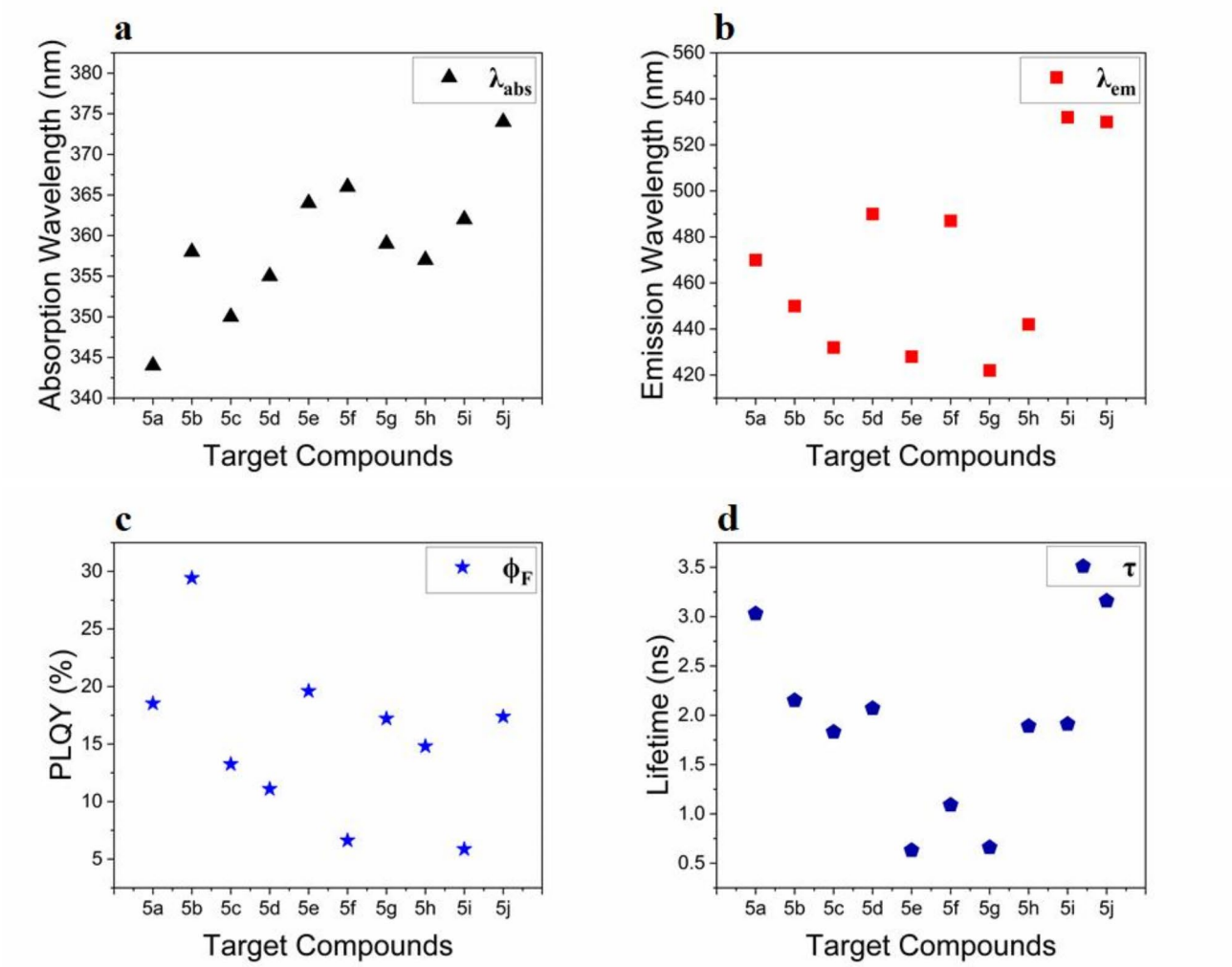


**Fig. 6**. Variations of (**a**) absorption maximum, (**b**) emission maximum, (**c**) absolute PLQY, and (**d**) fluorescence lifetime of **5a-j** (film).

values of **5a-j** slightly decreased compared to $\Delta E_s$. The $\Delta E_F$ of **5a-j** is in the range of 3.79 to 3.96 eV; **5j** has the least $\Delta E_F$ (3.79 eV), and the other compounds have increasing $\Delta E_F$ values of 3.80 eV (**5b**), 3.82 eV (**5f**), 3.85 eV (**5a**), 3.88 eV (**5d** and **5h**), 3.89 eV (**5i**), 3.90 eV (**5c**), 3.94 eV (**5e**), and 3.96 eV (**5g**), respectively. The $\Delta E_s$ and $\Delta E_F$ values are not congruent, and factors such as molecular interaction (H-bonding, π-π stacking, etc.), molecular packing, film thickness, structure planarity, etc., shape the optical properties of thin films. According to the ground-state optimised structures (**SI** Fig. 4), structural planarity varies from compound to compound. This variation in planarity can lead to differences in inter- and intramolecular interactions and molecular packing, which ultimately contributes to the lack of a clear trend in the increase or decrease of $\Delta E_F$ values. However, the $\Delta E_F$ values indicate the impact of bandgap engineering in thin film samples as well. Variations in structural planarity among the compounds affect intermolecular interactions and packing, leading to distinct electronic environments and $\Delta E_F$. This highlights how bandgap tuning in thin films can be achieved through careful manipulation of molecular structure and arrangement, even if a consistent trend is not observed across the different derivatives studied here.

According to Fig. 5b, the $\lambda_{em}$ is located in the range of 422 to 532 nm, and the emission band is broader to the extent of 220 to 300 nm and covers the violet-green region of visible light. Similar to the UV-visible peak, the films' redshifted $\lambda_{em}$ and broader emission peak (**5a-j**) can be attributed to factors such as molecular aggregation, molecular packing, intermolecular interactions (π-π stacking), restricted molecular motions, etc. On account of the CIE plot corresponding to the film state emission data (Fig. 5c), the emission colour of **5a-j** is in the blue-green region. When compared to the solution phase, the emission colour is drastically changed in the solid phase, which also confirms the dual-state emission of the proposed fluorophore class. The absolute $\phi_F$ and τ of the film samples were also measured, and the values lie between 5.86% and 29.43%. The compounds **5b** (29.43%), **5e** (19.6%), **5a** (18.52%), **5j** (17.38%), **5g** (17.21%), and **5h** (14.8%) displayed a moderate $\phi_F$, and their satisfactory emission efficiency and versatility allow them to be used effectively in imaging, sensing, optoelectronic devices, etc. For the majority of compounds, the values of $\phi_F$ are being lowered compared to solution-phase results. This may be due to molecular aggregation in the solid phase (thin film), leading to a fluorescence quenching

| Compound | UV $\lambda_{abs}$ (nm) | Excitation (nm) | PL $\lambda_{em}$ (nm) | $\lambda_{Onset}$ (nm) | $\Delta E_F$ (eV) | CIE (u', v') | $\phi_F$ (%) | τ (ns) |
|---|---|---|---|---|---|---|---|---|
| **5a** | 344 | 350 | 470 | 412 | 3.85 | 0.13, 0.39 | 18.52 | 3.03 |
| **5b** | 358 | 355 | 450 | 437 | 3.80 | 0.14, 0.30 | 29.43 | 2.15 |
| **5c** | 350 | 350 | 432 | 400 | 3.90 | 0.13, 0.31 | 13.25 | 1.83 |
| **5d** | 355 | 355 | 490 | 411 | 3.88 | 0.18, 0.48 | 11.09 | 2.07 |
| **5e** | 364 | 360 | 428 | 412 | 3.94 | 0.14, 0.32 | 19.6 | 0.63 |
| **5f** | 366 | 365 | 487 | 420 | 3.82 | 0.15, 0.49 | 6.62 | 1.09 |
| **5g** | 359 | 360 | 422 | 423 | 3.96 | 0.16, 0.29 | 17.21 | 0.66 |
| **5h** | 357 | 350 | 442 | 430 | 3.88 | 0.15, 0.35 | 14.8 | 1.89 |
| **5i** | 362 | 360 | 532 | 444 | 3.89 | 0.16, 0.51 | 5.86 | 1.91 |
| **5j** | 374 | 370 | 530 | 469 | 3.79 | 0.16, 0.53 | 17.38 | 3.16 |

**Table 3**. The overall photophysical characteristics of **5a-j** (thin film).

mechanism. In solution, the polarity of solvents can stabilise the formed excitons and reduce the non-radiative pathway, whereas, in thin films, a lack of stabilising medium can make the excitons more susceptible to non-radiative decay[35]. Figure 5d displays the measured fluorescence lifetime of **5a-j**, which ranges from 0.63 to 3.16 ns. Table 3 provides a summary of

the overall photophysical characteristics of compounds **5a-j** (thin film). The variations in absorption maximum, emission maximum, absolute PLQY, and fluorescence lifetime among **5a-j** (thin film) are portrayed in Fig. 6a-d.

According to the comprehensive photophysical studies, the unique optical characteristics of **5a-j** in solution phase (DMF) and solid phase (thin film) are revealed. Changing the aromatic substituents at the 4$^{th}$ and 6$^{th}$ positions of the 2-aminopyrimidine core/ plug-and-play design strategy has significantly influenced the optical characteristics of **5a-j**. The local environmental factors (presence and absence of solvents), the concentration of fluorophores in the solution phase, the possibility of molecular motion and rotation in dilute solution, restricted molecular rotation in the solid phase, effective π-π stacking in the solid phase, etc., led to distinctive results in solution phase and solid phase. The theoretically calculated bandgap (ΔE) values are in good agreement with experimental results ($\Delta E_s$). Figures 4 and 6 highlight the customisable optical properties of fluorophores **5a-j** both in solution and solid phase, thereby confirming their dual-state emission ability. Promising $\phi_F$ displayed by **5b** (71.00%), **5a** (59.26%), and **5c** (57.60%) in DMF imply that the fluorophore exhibits great efficiency in re-emitting more than 50% of the absorbed photons as fluorescence. This high fluorescence efficiency is a key feature that makes these compounds valuable for future research and practical applications. Similarly, the film samples of a few compounds displayed a moderate $\phi_F > 15\%$ [**5b** (29.43%), **5e** (19.6%), **5a** (18.52%), **5j** (17.38%), and **5g** (17.21%)], which is very considerable for solid-state emissive applications like OLEDs. The distinctive dual-state emission characteristics of the target compounds make them well-suited for use in a wide range of domains, including optoelectronics, biomedical imaging, and chemical sensors, among numerous others. To sum up, we could successfully present the first dual-state emissive fluorophores from a 2-aminopyrimidine core with a tunable molecular architecture, synthesised through simple chemistry, and most importantly, display good quantum yield/$\phi_F$ both in solution and solid phases.

## Electrochemical studies

The electrochemical investigations were conducted on a CV workstation with a three-electrode combination setup in a supporting electrolyte solution at room temperature. A glassy carbon-working electrode, an Ag/AgCl (sat. KCl) reference electrode, and a platinum wire-counter electrode were employed. The electrochemical cell was immersed in a 0.1 M tetrabutylammonium hexafluorophosphate ($NBu_4PF_6$) solution in acetonitrile, which served as the supporting electrolyte. The calibration of the electrochemical cell was performed using the ferrocene reference system. The target compounds **(5a-j)** with a concentration of $1 \times 10^{-3}$ M in acetonitrile were used in the aforementioned system to get the cyclic voltammogram. The scan rate employed was 50 mV/s, and the potential window ranged from −3 V to +3 V. Figure 7 represents the recorded cyclic voltammogram of the compounds **5a-j**. The first oxidation peak of the studied compounds is located between 1.72 and 2.44 eV, and the reduction peaks observed in the negative potential region are similar to the peaks present in the voltammogram of the supporting electrolyte (**SI Fig. 12**). From the oxidation onset potential and optical bandgap ($\Delta E_s$), the HOMO and LUMO energy ($E_{HOMO}$ and $E_{LUMO}$) of the target compounds were calculated using the below equation (I), and the overall electrochemical behaviour of **5a-j** is summarised in Table 4. Most interestingly, the experimentally calculated HOMO and LUMO energy values are in comparable agreement with the theoretically calculated results. Hence, the possibility of engineering the HOMO/LUMO energy levels of 2-aminopyrimidines by varying the aryl rings at the 4$^{th}$ and 6$^{th}$ positions is also established from the CV studies and provides the best proof for the distinctive electronic environment of each target compound.

$E_{HOMO} = -[E_{Onset}\ Ox + 4.4]$ .....(I).

$E_{LUMO} = E_{HOMO} + \Delta E_s$

$E_{Ox}$ – Oxidation potential, $E_{Onset}$ Ox – Oxidation onset potential

## Conclusion

In this study, we successfully explored the optical and electronic properties of 4,6-diarylpyrimidin-2-amine derivatives, a class of heterocyclic aromatic compounds best known for their biological relevance but least considered based on their photophysical and electrochemical characteristics. By adopting a novel plug-and-play approach, we designed and synthesised ten fluorophores **(5a-j)** featuring a 2-aminopyrimidine core and having diverse aryl substituents at the 4$^{th}$ and 6$^{th}$ positions. These derivatives were obtained with moderate to good yields (54–74%), and their structures were confirmed through comprehensive spectroscopic techniques (IR, NMR, and HRMS) and single-crystal XRD analysis. Our design strategy, which focuses on tuning the aromatic substituents, proved highly effective in achieving distinct optical properties, as confirmed by both experimental and computational studies. The theoretically calculated bandgap (ΔE) values are in good agreement with experimental results ($\Delta E_s$). Notably, the photophysical studies revealed dual-state emission behaviour for **5a-j** both in the solution and solid phases, with compounds such as **5b** (71.00%), **5a** (59.26%), and **5c** (57.60%) showing high quantum yields ($\phi_F$) in DMF, and these along with several other derivatives (**5b**, **5e**, **5a**, **5j**, and **5g**) exhibiting moderate quantum yields (> 15%) when used as thin films. Their emission efficiency and CIE coordinates highlight the versatility of these compounds as promising fluorescent emitters. The fluorescence lifetimes of **5a-j**, ranging from 0.8 to 1.5 ns in solution and 0.63 to 3.16 ns in thin films, further support their potential as efficient emitters.

The distinctive optical properties observed in both phases are attributed to environmental factors such as molecular rotation in solution and π-π stacking interactions in the solid phase, highlighting the value of these dual-state emissive materials. Electrochemical studies using cyclic voltammetry demonstrated the tunability

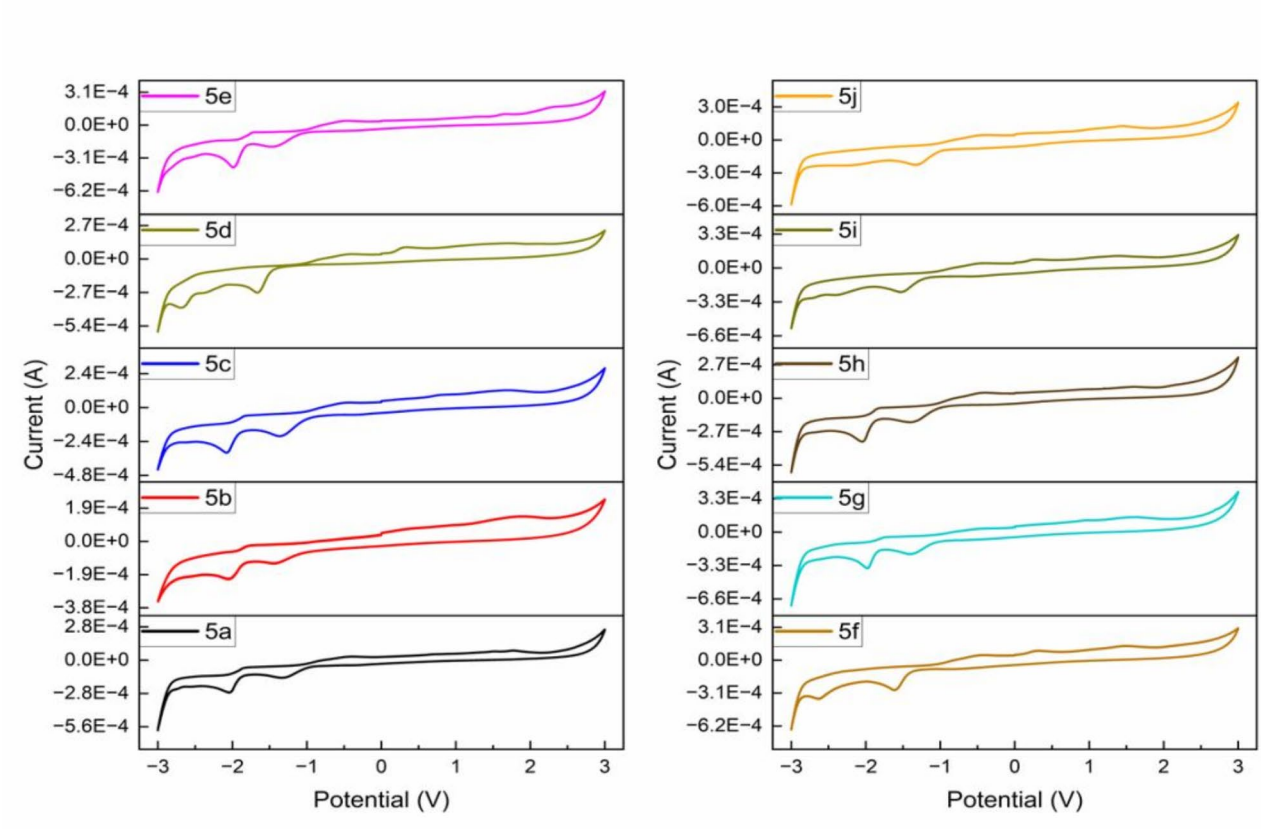


**Fig. 7**. Cyclic voltammogram of **5a-j**.

| Compound | $E_{Ox}$ (V) | $E_{Onset}$ Ox (V) | $E_{HOMO}$ (eV) | $\Delta E_s$ (eV) | $E_{LUMO}$ (eV) |
|---|---|---|---|---|---|
| **5a** | 1.77 | 1.65 | −6.05 | 4.37 | −1.68 |
| **5b** | 1.83 | 1.68 | −6.08 | 3.94 | −2.14 |
| **5c** | 1.72 | 1.63 | −6.03 | 4.09 | −1.94 |
| **5d** | 2.11 | 1.85 | −6.25 | 4.15 | −2.10 |
| **5e** | 2.21 | 1.84 | −6.24 | 4.03 | −2.21 |
| **5f** | 2.34 | 1.88 | −6.28 | 3.97 | −2.31 |
| **5g** | 2.44 | 1.95 | −6.35 | 4.03 | −2.32 |
| **5h** | 2.16 | 1.92 | −6.32 | 4.08 | −2.24 |
| **5i** | 2.23 | 1.95 | −6.35 | 4.05 | −2.30 |
| **5j** | 2.15 | 1.82 | −6.22 | 3.97 | −2.25 |

**Table 4**. Electrochemical properties of **5a-j**.

of the HOMO/LUMO energy levels through variation of the aryl substituents, offering a pathway for further electronic property optimisation. The reactive amino group in these derivatives also presents opportunities for future structural modification, enhancing their applicability in optoelectronic systems. In conclusion, we have demonstrated the first dual-state emissive fluorophores based on a 2-aminopyrimidine core, combining flexible molecular design with excellent emission efficiency. These findings pave the way for further exploration of these compounds both in solution and solid-phase applications, and we anticipate their potential to be further developed for advanced practical uses.

## Experimental section

### Materials and methods

The present study used pure reagents and chemicals, purchased from Sigma Aldrich and Avra Synthesis Pvt. Ltd., for synthesis and analysis. The melting point of the compounds was determined using digital melting point equipment. $^{1}H$ and $^{13}C$ NMR spectra were obtained using an FT-NMR spectrometer System-400 MHz, with TMS as the internal standard and $CDCl_3$ as the solvent. HRMS spectra were acquired using the HRMS-ESI + ve

mode on a WATERS XEVO G2-XS-QToF mass spectrometer. Single crystal XRD analysis was performed on a Bruker Kappa Apex II instrument, and the molecular packing and intermolecular interactions were elucidated using CCDC Mercury software, version no: Mercury 2024.2.0 (Build 415171) (https://www.ccdc.cam.ac.uk/solutions/software/free-mercury/). UV-visible and photoluminescence spectra were recorded using the Shimadzu UV-2600 UV-Vis Spectrophotometer and the LS 55 PerkinElmer Spectrophotometer. A 0.1 mM concentration of compounds **5a-j** in DMF solvent was used for solution state absorption and emission studies. The compounds **5a-j** were dissolved in DMF solvent (concentration ≈ 0.1 M), and the prepared solutions (50 µL) were evenly drop casted into round glass slides (diameter: 12 mm, thickness: 0.15 mm). The glass slides were kept for slow drying in the same solvent atmosphere for 1 week to obtain the thin films of the target compounds. The optical microscope image of the drop casted films was captured using a Stereo Zoom Microscope Zeiss Stemi 508 Trino with camera attachment, which confirmed the film formation and surface uniformity (**SI Fig. 13**). Electrochemical investigations were performed using a Metrohm Autolab potentiostat-galvanostat system. Theoretical calculations were performed using Gaussian09W software, version Gaussian09W Revision C.01 for 64-bit (https://gaussian.com/glossary/g09/), and optimised structures were visualised using GaussView 5.0. DFT (Density Functional Theory) with the B3LYP method and the 6–31 + g(d, p) basis set were used to describe the target compound structure using optimisation and FMOs[36].

## Synthesis

The designed compounds were synthesised by reacting a set of known chalcones[16,37–44]with guanidine hydrochloride[45,46]. The required chalcones were synthesised *via* the well-known base-catalysed Claisen-Schmidt condensation process of chosen aldehydes and ketones[47]. The structure of all the synthesised compounds was confirmed using advanced spectroscopic techniques (IR, $^{1}$H NMR, $^{13}$C NMR, and HRMS).

*General synthesis of chalcones (3aa, 3ba, 3ca, 3da, 3bb, 3bd, 3cc, 3cb, 3cd, and 3dd)*

The mixture of 1 eq. of ketone (**1a-d**) and 1 eq. of aldehyde (**2a-d**) in ethanol (10% w/v) was initially stirred for 5 min, followed by the addition of 10% KOH solution (1.5 eq.). TLC was used to monitor the reaction progress in an 8:2 hexane-ethyl acetate solvent system, with stirring continued for 20–24 h at room temperature. After reaction completion, ethanol is distilled off, and the obtained crude mass is extracted with ethyl acetate. The combined ethyl acetate layer was dried with anhydrous sodium sulphate, and the solvent was concentrated under vacuum. The obtained crude mixture was purified by silica gel column chromatography (100–200 mesh size) with hexane-ethyl acetate solvent mixtures to get the required chalcone derivatives in 79–94% yield. The synthesis scheme of chalcone derivatives is shown in Fig. 8a.

*General synthesis of 4, 6-diarylpyrimidin-2-amines (5a-j)*

To obtain the target compounds **5a-j**, 1 eq. of the synthesised chalcone (**3aa**, **3ba**, **3ca**, **3da**, **3bb**, **3bd**, **3cc**, **3cb**, **3cd**, and **3dd**) and 2 eq. guanidine hydrochloride **4** was dissolved in ethanol (10% w/v) and stirred for 5 min. To the stirring reaction mixture, 20% KOH (2.5 eq.) was added dropwise and refluxed for 4–6 h. TLC was used to monitor the reaction progress in an 8:2 hexane-ethyl acetate solvent system. After the reaction was completed, ethanol was distilled off, and the obtained crude mass was extracted with ethyl acetate. The combined ethyl acetate layer was dried with anhydrous sodium sulphate, and the solvent was concentrated under vacuum. The

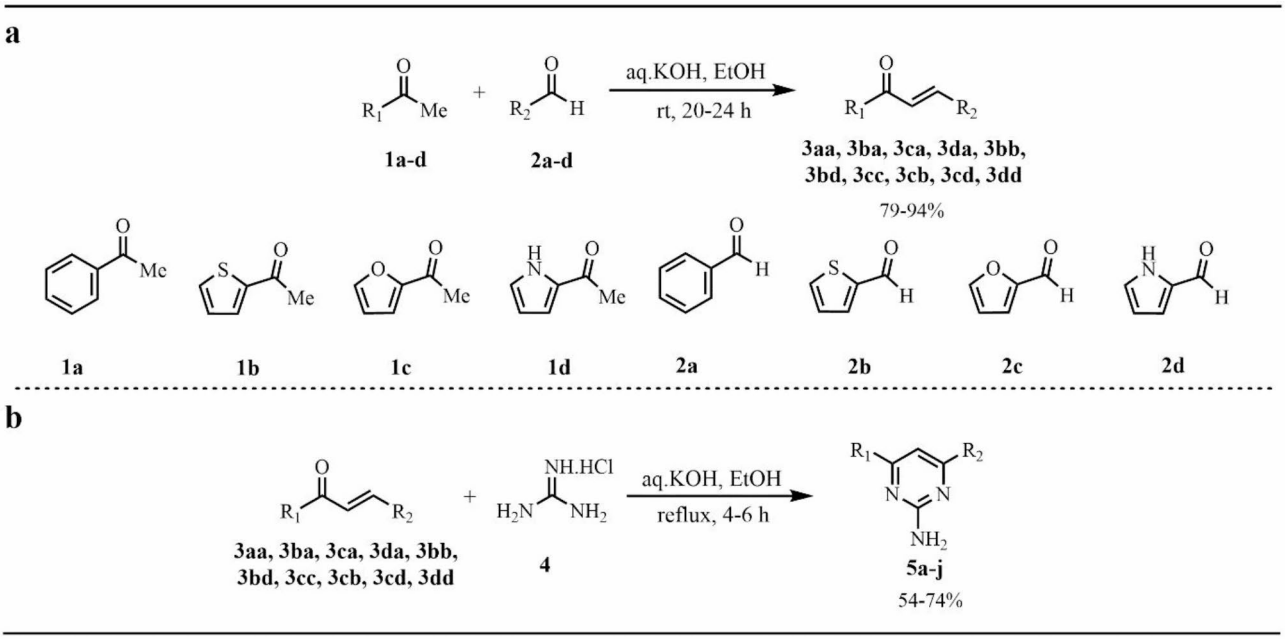


**Fig. 8**. The synthesis scheme of compounds **3** and **5a-j**.

crude product was purified using silica gel column chromatography (100–200 mesh size) using a hexane-ethyl acetate solvent system, yielding 54–74% of 4, 6-diarylpyrimidin-2-amine (**5a-j**) derivatives. Figure 8b represents the synthesis scheme of **5a-j**. The reaction time, physical properties, yield, and structure characterisation results of compounds **3** and **5a-j** are summarised in the **SI** Tables 4 and 5, and their IR, NMR, and HRMS spectra are displayed in the SI section (**SI Figs. 14, 15, 16, 17, 18, 19, 20, 21, 22, 23, 24, 25, 26, 27, 28, 29, 30, 31, 32, 33, 34, 35, 36, 37, 38, 39, 40, 41, 42, 43, 44, 45, 46, 47, 48, 49, 50, 51, 52, 53, 54, 55, 56, 57, 58, 59, 60, 61, 62, 63 and 64**), respectively.

## Data availability

The datasets used and/or analysed during the current study available from the corresponding author on reasonable request.

Received: 5 August 2024; Accepted: 28 November 2024
Published online: 30 November 2024

## References

1. Valeur, B. & Berberan-Santos M. N. A brief history of fluorescence and phosphorescence before the emergence of quantum theory. *J. Chem. Educ.* **88**, 731–738 (2011).
2. Yang, Y. et al. Fluorescent organic small molecule probes for bioimaging and detection applications. *Molecules* **27**, 8421 (2022).
3. Baeyer, A. & Drewsen, V. Darstellung Von indigblau aus orthonitrobenzaldehyd. *Ber Dtsch. Chem. Ges.* **15**, 2856–2864 (1882).
4. Yu, T., Liu, L., Xie, Z. & Ma, Y. Progress in small-molecule luminescent materials for organic light-emitting diodes. *Sci. China Chem.* **58**, 907–915 (2015).
5. Ha, J. M., Hur, S. H., Pathak, A., Jeong, J. E. & Woo, H. Y. Recent advances in organic luminescent materials with narrowband emission. *NPG Asia Mater.* **13**, 53 (2021).
6. Li, Y., Liu, T. & Sun, J. Recent advances in n-heterocyclic small molecules for synthesis and application in direct fluorescence cell imaging. *Molecules* **28**, 733 (2023).
7. Biswas, S., Gangopadhyay, M., Barman, S., Sarkar, J. & Singh, N. D. P. Simple and efficient coumarin-based colourimetric and fluorescent chemosensor for $F^-$ detection: an $ON^1$-OFF-$ON^2$ fluorescent assay. *Sens. Actuators B: Chem.* **222**, 823–828 (2016).
8. Zheng, Q. et al. Ultra-stable organic fluorophores for single-molecule research. *Chem. Soc. Rev.* **43**, 1044–1056 (2014).
9. Chen, Y. et al. Determining essential requirements for fluorophore selection in various fluorescence applications taking advantage of diverse structure–fluorescence information of chromone derivatives. *J. Med. Chem.* **64**, 1001–1017 (2020).
10. Sreekumar, A. et al. Thiophene-centered small molecule emitters. *AIP Conf. Proc.* 3171, 020001 (2024).
11. Ullah, F. et al. Fluorescent and phosphorescent nitrogen-containing heterocycles and crown ethers: biological and pharmaceutical applications. *Molecules* **27**, 6631 (2022).
12. Papucci, C. et al. Green/yellow-emitting conjugated heterocyclic fluorophores for luminescent solar concentrators. *Eur. J. Org. Chem.* 2657–2666 (2018). (2018).
13. Li, W., Feng, W., Liu, B. & Qian, Y. Fluorescent protein chromophores modified with aromatic heterocycles for photodynamic therapy and two-photon fluorescence imaging. *Org. Biomol. Chem.* **22**, 1892–1900 (2024).
14. Kumar, S. et al. Synthesis, crystal structure, spectroscopic characterization, hirshfeld surface analysis, DFT calculation and molecular modeling studies of 1-(4-Nitro-phenyl)-3,5-di-thiophen-2-yl-1H-pyrazole. *Mol. Cryst. Liq Cryst.* **740**, 35–53 (2022).
15. Nair, A. R., Kumar, Y. S. & Sivan, A. Synthesis and in-depth investigation of the photophysical and electrochemical properties of novel pyrazole cored D-A-D molecules. *Opt. Mater.* **134**, 113117 (2022).
16. Nair, A. R. et al. D-A-D/A chalcones with tunable optical characteristics: synthesis, photophysical, electrochemical and theoretical investigations. *J. Photochem. Photobiol A: Chem.* **451**, 115511 (2024).
17. Bettendorff, L. & Wins, P. in *Encyclopedia of Biological Chemistry*. 202–209 (eds Lennarz, W. J. & Lane, M. D.) (Elsevier, 2013).
18. Brown, D. J. in *Comprehensive Heterocyclic Chemistry*. 57–155 (eds Katritzky, A. R. & Rees, C. W.) (Elsevier, 1984).
19. Nammalwar, B. & Bunce, R. A. Recent advances in pyrimidine-based drugs. *Pharmaceuticals* **17**, 104 (2024).
20. Santos, P. L. et al. Use of pyrimidine and pyrazine bridges as a design strategy to improve the performance of thermally activated delayed fluorescence organic light emitting diodes. *ACS Appl. Mater. Interfaces.* **11**, 45171–45179 (2019).
21. Rodella, F. et al. Low efficiency roll-off blue TADF OLEDs employing a novel acridine–pyrimidine based high triplet energy host. *J. Mater. Chem. C.* **9**, 17471–17482 (2021).
22. Li, B. et al. Pyrimidine-based thermally activated delayed fluorescent materials with unique asymmetry for highly-efficient organic light-emitting diodes. *Dyes Pigm.* **203**, 110373 (2022).
23. Park, I. S., Komiyama, H. & Yasuda, T. Pyrimidine-based twisted donor–acceptor delayed fluorescence molecules: a new universal platform for highly efficient blue electroluminescence. *Chem. Sci.* **8**, 953–960 (2017).
24. Varga, L. et al. Solution-phase parallel synthesis of 4, 6-diaryl-pyrimidine-2-ylamines and 2-amino-5,5-disubstituted-3,5-dihydro-imidazol-4-ones via a rearrangement. *Tetrahedron* **59**, 655–662 (2003).
25. El-Rayyes, N. R. Heterocycles. Part I. A new route to the synthesis of substituted 2-aminopyrimidines. *J. Heterocycl. Chem.* **19**, 415–419 (1982).
26. Petrova, O. V. et al. Pyrrole–aminopyrimidine ensembles: cycloaddition of guanidine to acylethynylpyrroles. *Molecules* **26**, 1692 (2021).
27. Mughal, E. U. et al. Pyrimidine-based azo dyes: synthesis, photophysical investigations, solvatochromism explorations and antibacterial activity. *Dyes Pigm.* **220**, 111762 (2023).
28. Forero-Cortés, P. A. & Haydl, A. M. The 25th anniversary of the Buchwald–Hartwig Amination: Development, Applications, and Outlook. *Org. Process. Res. Dev.* **23**, 1478–1483 (2019).
29. Gengwei, L. et al. Improving electron mobility of tetraphenylethene-based aiegens to fabricate nondoped organic light-emitting diodes with remarkably high luminance and efficiency. *ACS Appl. Mater. Interfaces.* **8**, 16799–16808 (2016).
30. Xuejun, Z. et al. Polyphenylbenzene as a platform for deep-blue OLEDs: aggregation enhanced emission and high external quantum efficiency of 3.98%. *Chem. Mater.* **27**, 1847–1854 (2015).
31. Chunqiu, Z. et al. Cell membrane tracker based on restriction of intramolecular rotation. *ACS Appl. Mater. Interfaces.* **6**, 8971–8975 (2014).
32. Sijie, C. et al. Full-range intracellular pH sensing by an aggregation-induced emission-active two-channel ratiometric fluorogen. *J. Am. Chem. Soc.* **135**, 4926–4929 (2013).
33. Jiasheng, W., Weimin, L., Jiechao, G., Hongyan, Z. & Pengfei, W. New sensing mechanisms for design of fluorescent chemosensors emerging in recent years. *Chem. Soc. Rev.* **40**, 3483–3495 (2011).
34. Furniss, B. S., Hannaford, A. J., Smith, P. W. G. & Tatchell, A. R. Vogel's textbook of practical organic chemistry, fifth edition 1443–1445 (John Wiley & Sons, (1989).

35. Majid, A., Kiran, S., Sandhu, Q., Khan, S. & Khan, S. The effects of polar solvents on structural, electronic, and optical properties of organic dyes. *Int. J. Quantum Chem.* **122**, e26876 (2022).
36. Silvarajoo, S. et al. Dataset of theoretical molecular electrostatic potential (MEP), highest occupied molecular orbital-lowest unoccupied molecular orbital (HOMO-LUMO) band gap and experimental cole-cole plot of 4-(ortho-, meta- and para-fluorophenyl)thiosemicarbazide isomers. *Data Br.* **32**, 106299 (2020).
37. Adnan, D., Singh, B., Mehta, S. K., Kumar, V. & Kataria, R. Simple and solvent free practical procedure for chalcones: an expeditious, mild and greener approach. *Curr. Res. Green. Sustain. Chem.* **3**, 100041 (2020).
38. Nagwanshi, R., Bakhru, M. & Jain, S. Photodimerization of heteroaryl chalcones: comparative antimicrobial activities of chalcones and their photoproducts. *Med. Chem. Res.* **21**, 1587–1596 (2011).
39. Yang, F. et al. High efficiency photoinitiators with extremely low concentration based on furans derivative. *J. Photochem. Photobiol A: Chem.* **406**, 112994 (2021).
40. Gunasekharan, M. et al. Preliminary insight of pyrrolylated-chalcones as new anti-methicillin-resistant staphylococcus aureus (anti-mrsa) agents. *Molecules* **26**, 5314 (2021).
41. Stark, D. G. et al. Isothiourea-catalysed enantioselective pyrrolizine synthesis: synthetic and computational studies. *Org. Biomol. Chem.* **14**, 8957–8965 (2016).
42. Rámila, A., Plumet, J. & Camacho, E. A convenient approach to pentagonal 2,3':5',2-triheterocyclic compounds. *Heterocycles* **45**, 2425 (1997).
43. Kalmouch, A., Rdwan, M., Omran, M. M., Sharaky, M., Moustafa, G. O. & Synthesis of novel 2, 3'-bipyrrole derivatives from chalcone and amino acids as antitumor agents. *Egypt. J. Chem.* **63**, 4409–4421 (2020).
44. Tsukerman, S. V., Izvekov, V. P. & Lavrushin, V. F. Synthesis of chalcone analogs containing a pyrrole ring. *Chem. Heterocycl. Compd.* **1**, 352–354 (1966).
45. Farooq, S. & Ngaini, Z. One-pot and two-pot methods for chalcone derived pyrimidines synthesis and applications. *J. Heterocycl. Chem.* **58**, 1209–1224 (2021).
46. Kumar, N., Drabu, S. & Shalini, K. Synthesis and pharmacological screening of 4, 6-substituted di-(phenyl) pyrimidin-2-amines. *Arab. J. Chem.* **10**, S877–S880 (2017).
47. Abaee, M. S., Cheraghi, S., Navidipoor, S., Mojtahedi, M. M. & Forghani, S. An efficient tandem aldol condensation-thia-Michael addition process. *Tetrahedron Lett.* **53**, 4405–4408 (2012).


## Acknowledgements

The authors gratefully acknowledge support from the Department of Chemistry at Amrita Vishwa Vidyapeetham, Amritapuri campus. We gladly acknowledge Prof. Dr. Jayasree Elambalassery from Cochin University of Science and Technology, Kochi, Kerala, for her guidance in DFT studies. We appreciate Ms. Anu Mathew, SAIF, Mahatma Gandhi University, Kottayam, Kerala, for providing the fluorescence lifetime and quantum efficiency facility. We thank Dr. Shankara H. N. of Chromatogen Analytical Solutions (Mysore, Karnataka, India) for NMR and HRMS analysis.

## Author contributions

Ajil R. Nair: Writing – original draft, Methodology, Investigation, Formal analysis, Conceptualization. M. Gayathri Mohan: Formal analysis, Methodology. C. Raksha: Formal analysis, Methodology, Software. Anjana Sreekumar: Formal analysis, Methodology, Software. P. Manoj: Validation, Writing – review & editing. Sunil Kumar Y.C.: Writing – review & editing, Validation, Supervision. Akhil Sivan: Writing – review & editing, Validation, Supervision, Project administration, Methodology, Conceptualization.

## Declarations

## Competing interests

The authors declare no competing interests.

## Additional information

**Supplementary Information** The online version contains supplementary material available at https://doi.org/10.1038/s41598-024-81723-1.

**Correspondence** and requests for materials should be addressed to A.S.